Crystal structure of the yeast eIF4A-eIF4G complex: An RNA-helicase controlled by protein–protein interactions

Patrick Schütz*, Mario Bumann*†, Anselm Erich Oberholzer*‡, Christoph Bieniossek*§, Hans Trachsel¶, Michael Altmann¶‖, and Ulrich Baumann*‖

*Departement für Chemie und Biochemie, Universität Bern, Freiestrasse 3, CH-3012 Bern, Switzerland; and ¶Institut für Biochemie und Molekulare Medizin, Universität Bern, Bühlstrasse 28, CH-3012 Bern, Switzerland

Edited by Thomas A. Steitz, Yale University, New Haven, CT, and approved May 1, 2008 (received for review January 15, 2008)

Translation initiation factors eIF4A and eIF4G form, together with the cap-binding factor eIF4E, the eIF4F complex, which is crucial for recruiting the small ribosomal subunit to the mRNA 5′ end and for subsequent scanning and searching for the start codon. eIF4A is an ATP-dependent RNA helicase whose activity is stimulated by binding to eIF4G. We report here the structure of the complex formed by yeast eIF4G's middle domain and full-length eIF4A at 2.6-Å resolution. eIF4A shows an extended conformation where eIF4G holds its crucial DEAD-box sequence motifs in a productive conformation, thus explaining the stimulation of eIF4A's activity. A hitherto undescribed interaction involves the amino acid Trp-579 of eIF4G. Mutation to alanine results in decreased binding to eIF4A and a temperature-sensitive phenotype of yeast cells that carry a Trp579Ala mutation as its sole source for eIF4G. Conformational changes between eIF4A's closed and open state provide a model for its RNA-helicase activity.

translation initiation | DEAD-box protein | X-ray structure | eIF4F

Translation initiation in eukarya is usually the rate-limiting and most tightly controlled stage of polypeptide synthesis (reviewed in refs. 1–3). For the majority of eukaryotic mRNAs, the cap-dependent pathway is used for translation initiation (3). It comprises four consecutive steps: (*i*) formation of the 43S preinitiation complex consisting of the 40S ribosomal subunit, initiation factors (eIF2, eIF3), and Met-tRNA^{i}; (*ii*) recruitment of the 43S preinitiation complex to the capped 5′ end of the mRNA; (*iii*) scanning of the 5′ untranslated region of the mRNA and start codon recognition; and (*iv*) joining of the large 60S ribosomal subunit and assembly of the 80S ribosome.

Approximately a dozen eukaryotic translation initiation factors (eIFs) are needed for this process. A central component of the second and third step is eIF4F, a heterotrimeric stable complex consisting of the cap-binding protein eIF4E, the DEAD-box helicase eIF4A, and the central multiscaffold protein eIF4G, which possesses additional binding sites for the poly(A)-binding protein PABP and, in mammalia, for eIF3 (Fig. 1*A*). Mammalian eIF4G possesses a second eIF4A binding site in its C-terminal region in proximity to a binding site for protein kinase Mnk1 (mitogen-activated protein kinase-interacting kinase), which phosphorylates eIF4E. Crystal structures of the central and the C-terminal region of human eIF4GII reveal the formation of one or two HEAT domains, respectively (4, 5)

Saccharomyces cerevisiae possesses two genes encoding for eIF4G, TIF4631 and TIF4632. The gene products, eIF4GI and eIF4GII, are 952 and 914 aa long and share ≈50% sequence identity. Deletion of one of these genes is tolerated by yeast cells, but double deletion of both genes causes lethality. Interaction of eIF4G with eIF4A is essential for the cell (6, 7). The 45-kDa initiation factor 4A (eIF4A) is a prototypical DEAD-box helicase (8). Its ATPase activity is RNA-dependent and its activity is substantially enhanced in mammalian cells by eIF4B, eIF4H, and eIF4G (9–12). *S. cerevisiae* eIF4A is an essential, 395-aa-long protein encoded by a pair of duplicated genes, *TIF1* and *TIF2*. eIF4A is probably necessary for the translation of all mRNAs, presumably by unwinding mRNA secondary structures that could hinder the recruitment of 43S preinitiation complexes to the 5′ end and its subsequent scanning. Like other DEAD-box helicases, eIF4A possesses nine conserved sequence motifs, Q, I, Ia, Ib, II, III, IV, V, and VI (Fig. 1*B*), which are important for nucleotide and RNA binding and for helicase activity (13). The Q motif is responsible for the recognition of the adenine moiety of ATP (14–16). Motif I (also called Walker A) coordinates the α- and β-phosphate groups; Motif II (Walker B, DEAD) catalyzes ATP hydrolysis with the help of a glutamic acid residue, which acts as a catalytic base. The second and third arginine residues of Motif VI (IHRIGRGGR) probably function as an arginine finger, triggering ATP hydrolysis (17). Motif III couples ATP hydrolysis to RNA unwinding, whereas motifs Ia, Ib, IV, and V are proposed to participate in RNA binding and unwinding.

Crystal structures of full-length and of fragments of eIF4A have been determined (14, 18–20). Additionally, the structure of mammalian eIF4AIII, a structurally related but functionally different DEAD-box helicase, has been resolved in complex with other components of the exon junction complex (18, 21). All of these structures reveal two RecA-like domains that are connected by a flexible linker. In yeast, the N-terminal domain (NTD) of eIF4A comprises residues 1–220, and the C-terminal domain (CTD) residues 226–395. The DEAD-box sequence motifs are spread over both domains and nucleotide and RNA binding occurs in a cleft in between. Open and closed conformations for eIF4A and homologs depending on the nucleotide state have been described (19, 22, 23). The closed conformation, which is stabilized by ATP and RNA, is thought to catalyze ATP hydrolysis because the proper positioning of an arginine finger (motif VI) into the nucleotide-binding pocket (24, 25). ATP hydrolysis is presumed to trigger transition to the open conformation and the resulting mechanical force used for RNA unwinding.

Author contributions: M.B. and A.E.O. contributed equally to this work; H.T., M.A., and U.B. designed research; P.S., M.B., A.E.O., C.B., M.A., and U.B. performed research; P.S., M.B., A.E.O., C.B., M.A., and U.B. analyzed data; and M.A. and U.B. wrote the paper.

The authors declare no conflict of interest.

This article is a PNAS Direct Submission.

Data deposition: The atomic coordinates and structure factors have been deposited in Protein Data Bank, www.pdb.org (PDB ID codes 2VSX and 2VSO). .

†Present address: MRC France, CRG BM14 ESRF, B.P. 220, F-38043 Grenoble Cedex, France.

‡Present address: The Institute of Cancer Research, Section of Structural Biology, Chester Beatty Laboratories, Fulham Road, London SW3 6JB, United Kingdom.

§Present address: Institute of Molecular Biology and Biophysics, Schafmattstrasse 20, Swiss Federal Institute of Technology, CH-8093 Zürich, Switzerland.

‖To whom correspondence may be addressed. E-mail: michael.altmann@mci.unibe.ch or ulrich.baumann@ibc.unibe.ch.

This article contains supporting information online at www.pnas.org/cgi/content/full/0800418105/DCSupplemental.

© 2008 by The National Academy of Sciences of the USA

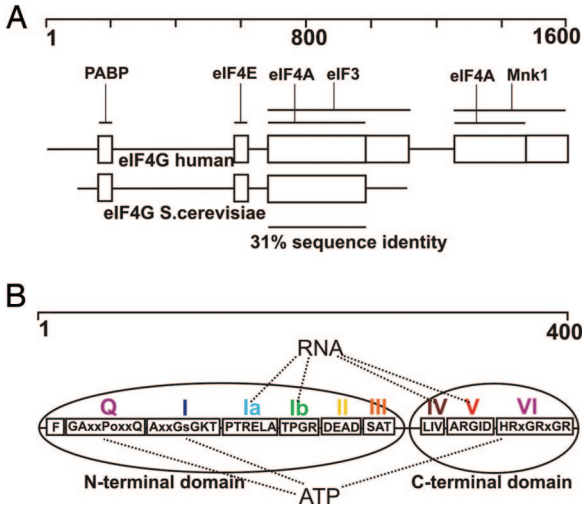

Fig. 1. Domain organization of eIF4G and eIF4A. (*A*) Schematic drawing of the domain organization of eIF4G and its binding sites. The scale bar indicates the amino acid positions. (*B*) Schematic drawing of eIF4A. The conserved sequence motifs of the DEAD-box helicase family are color-coded as follows: Q, magenta; Walker A/I, blue; Ia, cyan; Ib, green; Walker B/II, yellow; III, orange; IV, brown; V, red; and VI, magenta. The scale bar is very approximate; the N-terminal domain spans residues 1–221, the C-terminal domain residues 225–391.

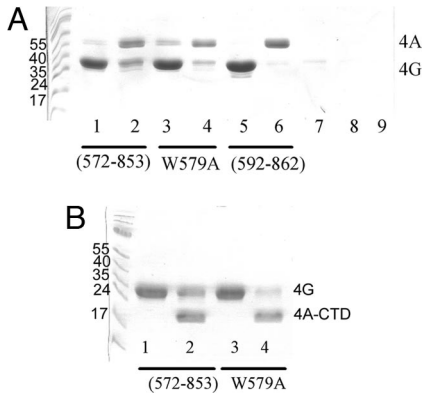

Fig. 2. Pull-down experiments using His-tagged yeast eIF4A in conjunction with yeast eIF4GI. His-tagged full-length eIF4A (*A*) or eIF4A-CTD (*B*) was bound to a Ni-NTA column. eiF4G proteins (10× excess) were added and incubated for 5 min. After washing out unbound proteins with 3 × 10 volumes of buffer, bound proteins were specifically eluted with 100 mM imidazole, separated on 15% SDS gels, and visualized by Coomassie staining. (*A*) Binding to full-length eIF4A. Markers: 1, eIF4G (572–853) wash; 2, eIF4G (572–853) elution; 3, eIF4G (572–853)(W579A) wash; 4, eIF4G (572–853)(W579A) elution; 5, eIF4G (592–862) wash; 6, eIF4G (592–862) elution; 7, 8, and 9, unspecific (background) adsorption of eIF4G proteins added to Ni-NTA columns in the absence of eIF4A. (*B*) Binding to eIF4A-CTD. Markers: 1, eIF4G (572–853) wash; 2, eIF4G (572–853) elution; 3, eIF4G (572–853)(W579A) wash; and 4, eIF4G (572–853)(W579A) elution.

Although several 3D structures of individual components of the translation initiation machinery have been resolved (26, 27), there is a lack of information of the structural features of protein–protein interactions at the atomic level. A number of reports have addressed the eIF4A–eIF4G interaction by isolating and characterizing mutants (6, 7, 28–31). An NMR study mapping the interaction sites of the human eIF4AI–eIF4GII complex has been published, but no atomic model has been proposed yet (10). To gain a deeper understanding of this essential protein–protein interaction, we determined the crystal structure of *S. cerevisiae* eIF4GI middle domain (residues 572–853) in a complex with full-length eIF4A.

Results

eIF4A and eIF4G (572–853) Form a Stable Complex with Increased ATPase Activity. A *TIF4631* fragment spanning residues 542–883 that still binds to eIF4A has been described (6). To find crystallizable fragments, we examined the binding of various engineered eIF4G proteins with full-length eIF4A or eIF4A-CTD. Gel filtration and pull-down experiments revealed that a shortened eIF4G (572–853) protein still binds to full-length eIF4A as a 1:1 complex, as confirmed by quantitative amino analysis of the peak fraction [Fig. 2; see also supporting information (SI) Fig. S1*A*]. For free eIF4A, the ATPase activity was estimated to ≈2.1 mol of P_i per mol of eIF4A and minute in a reaction mixture containing 1.0 μM purified eIF4A, 0.8 mg/ml poly(U) and 2.5 mM ATP at room temperature. To test for eIF4G's influence on eIF4A's ATPase activity, the same assay was performed in the presence of 2.0 μM different eIF4G proteins (Fig. 3). Yeast eIF4G (572–853) enhanced eIF4A's ATPase activity by more than threefold (Fig. 3*A*, lane 2). Further N-terminal shortening of eIF4G by 20 residues, as with yeast eIF4G (592–862) protein, significantly weakened binding to eIF4A (Fig. 2*A*, lanes 5 and 6) and this truncated construct consequently only enhances eIF4A's ATPase activity by ≈20% (Fig. 3*A*, lane 6). Although lacking ATPase activity, the eIF4A-CTD domain shows approximately the same affinity for eIF4G as full-length eIF4A (Fig. 2*B*, lanes 1 and 2; Fig. S1*B*).

We also examined the complex formation of human full-length eIF4A and two human eIF4GI proteins. Human eIF4GI (710–1056), which corresponds to yeast eIF4G (572–853) (see also Fig. S2), stimulates the ATPase activity of human eIF4AI also by a factor of three (Fig. 3*B*). However, human eIF4GI (710–970), a C-terminally shortened version lacking the last helix α10 (Fig. S2) still forms a stable complex (Fig. S1*F*) but only weakly enhances ATPase activity by ≈20% (Fig. 3*B*).

From these data we conclude that the interaction with helix α10 of eIF4G is an important element for stimulation of eIF4A's ATPase activity but dispensable for the formation of a stable complex.

Structure of Yeast eIF4A–eIF4G (572–853) Complex. The complex structure eIF4A–eIF4G (572–853) was determined in a monoclinic and in a triclinic crystal form at 2.8- and 2.6-Å resolution, respectively (Table S1). Structures were refined to R/R_{free} of 0.217/0.267 and 0.253/0.287, respectively. According to MolProbity (32), >95% (triclinic form) and 96% (monoclinic form) of all residues are in the favored Ramachandran regions, four residues (0.5%) are outliers.

Initial crystals were obtained in the monoclinic space group $P2_1$. Addition of AMP and ADP improved the crystal quality,

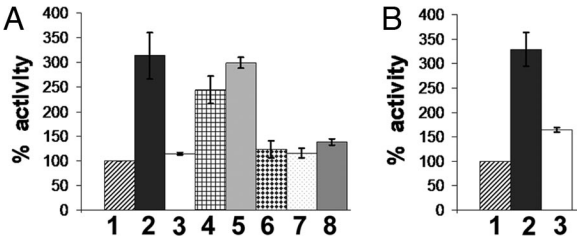

Fig. 3. Stimulation of eIF4A's ATPase activity by various eIF4G proteins. eIF4A was incubated in the absence or presence of 2.5-fold excess eIF4G protein and ATP and RNA at 22°C by using EnzChek phosphate assay. Phosphate release was measured for 15min. (*A*) Activity of yeast eIF4A (wild-type and mutant). 1, eIF4A + buffer (negative control); 2, eIF4A + eIF4G (572–853); 3, eIF4A(R35D) + buffer; 4, eIF4A(R35D) + eIF4G (572–853); 5, eIF4A + eIF4G (572–853)(D842R); 6, eIF4A + eIF4G (592–862); 7, eIF4A + eIF4G (572–853)(W579A); and 8, eIF4A + human eIF4G(710–1056). (*B*) Activity of human eIF4A in the presence of: 1, buffer; 2, human eIF4GI(710–1056); and 3, human eIF4GI (710–970).

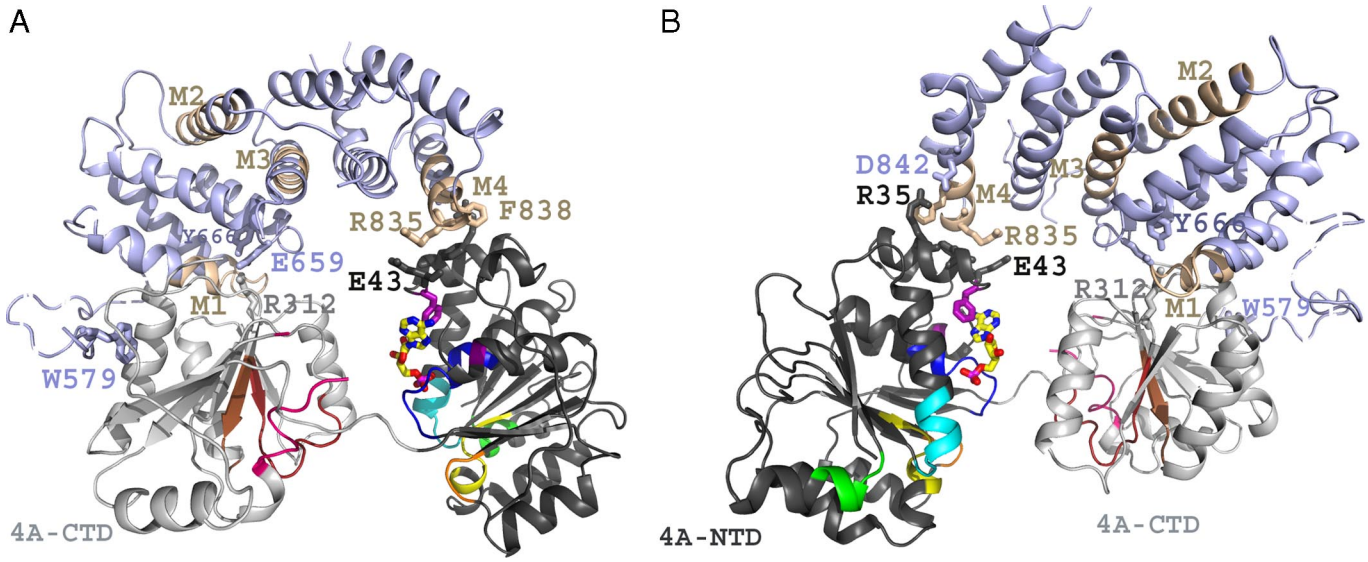

Fig. 4. Overall structure of the eIF4G–eIF4A complex. (*A*) Ribbon diagram of the x-ray structure of the complex. eIF4A is shown at the bottom in dark gray and light gray for the N-terminal and C-terminal domain, respectively. DEAD-box motifs are color-coded as follows: Q, magenta; Walker A/I, blue; IA, cyan; IB, green; Walker B/II, yellow; III, orange; IV, brown; V, red; and VI, magenta. AMP is shown as yellow sticks. eIF4G (572–853) is shown at the top and is colored in light blue; motifs M1–M4 are shown in tan. Some key residues mentioned in the text are shown as sticks. The dashed loop from eIF4G residues 582 to 600 (*Left*, blue) is modeled. (*B*) View rotated around the vertical by ≈180°. The salt bridge between eIF4A-NTD Arg-35 and eIF4G Asp-842 is indicated (*Upper Left*).

with AMP being the more effective. Because both additives produced isomorphous crystals we conclude that the conformation of eIF4A in these crystals corresponds to the *apo* or ADP form. For ADP- and AMP-bound eIF4A–eIF4G complexes, limited proteolysis gave identical degradation patterns, which were subtly different from the AMPPNP/RNA form (Fig. S3). Crystal annealing transformed the lattice to a triclinic structure with improved diffraction properties. The asymmetric unit of both crystal forms contains two virtually identical eIF4A–eIF4G complexes. There are also no significant differences between both crystal forms, the rms deviation for all Cα atoms is ≈0.2 Å. The segment containing eIF4G's residues 583–597 is not visible in the electron density map and neither are its loops 717–736 or 801–810. For eIF4A, amino acids 126–135 and 352–356 are disordered.

eIF4G (572–853) belongs to the HEAT-repeat protein family and contains 10 α-helices that form a right-handed solenoid (Fig. 4). Its convex surface interacts with both N- and C-terminal domains of eIF4A. The rms deviation to the human eIF4G-II middle domain (PDB ID code 1HU3) is 2.5 Å for 170 Cα atoms (5). The two structures differ most in position and length at their N-terminal four helices. This finding is remarkable because this part of eIF4G makes the strongest contacts to eIF4A-CTD. This could hint, on one hand, at induced-fit motions; on the other, it might explain why mouse eIF4A cannot complement the yeast factor (33) and why human eIF4GI (710–1056) does not stimulate yeast eIF4A ATPase activity (Fig. 3*A*, lane 8).

eIF4G (572–853) contacts the N- and C-terminal domains of eIF4A (eIF4A-NTD, eIF4A-CTD) and hence fixes the relative orientation of these with respect to each other (Fig. 4). eIF4A is in an open, dumbbell-shape conformation with the linker between the two RecA-like domains being visible in the electron density map. The extended conformation differs considerably from previously reported open conformations for apo-yeast eIF4A (PDB ID code 2FUU) (19) and for the human apo-eIF4AIII-Btz complex (PDB ID code 2JOU) (21) or apo-eIF4AIII (PDB ID code 2HXY) (18). A simple rigid-body superimposition with those structures results in rms values of all equivalent Cα atoms between 12 and 18 Å. These large deviations arise essentially from the different arrangements of eIF4A-NTD and eIF4A-CTD because separate superposition of NTD and CTD reduces these values to ≈1 Å. For example, compared with the *apo*-eIF4AIII-Btz, the two domains are rotated against each other by 175° in the eIF4A–eIF4G complex. Because of their different arrangement the conserved DEAD-box sequence motifs face each other and the active-site cleft between the two domains (Fig. 4*A*), whereas in previously reported structures they are twisted in relationship to each other. This is functionally important because RNA and ATP bind within the active-site cleft. Hence, eIF4G restricts eIF4A's conformation in such a way that important sequence motifs remain in a close spatial neighborhood and proper orientation, even in the open conformation.

The Interface. Although total contact area measures ≈1,500 Å^2, ≈2,900 Å^2 of accessible surface from both polypeptide chains become buried on complex formation. As expected from gel filtration and pull-down experiments, eIF4A-CTD shows the strongest interactions with eIF4G, burying ≈2,400 Å^2, whereas the contacts to eIF4A-NTD shield a total of 540 Å^2 of accessible surface. The interface contains 23 hydrogen bonds and 14 salt bridges. Although contact residues of eIF4G (572–853) with eIF4A-CTD are located on its N-terminal four helices and connecting loops, eIF4A's interacting amino acids reside mostly in loops that bridge helices and β-strands. The beginning of the last α-helix of eIF4G (572–853) establishes the contact to the first two helices in eIF4A's N-terminal domain.

Imataka and Sonenberg (28) have identified four sequence motifs (M1 to M4) in eIF4G that are considered to be important for the interaction with eIF4A . However, some of the mutations occur in the hydrophobic core of eIF4G, which does not interact with eIF4A, for example, in motifs M2 (residues 694–708 in yeast) or M3 (residues 744–753) (see also Fig. S2).

The largest contiguous interaction surface involves the C-terminal end of eIF4G (572–853)'s first helix, which carries the conserved M1 611-KSLLNKLTLEMF-622 motif (Fig. 4 and Fig. S2). The triple human eIF4GI mutant LLF614,617,622AAA (the numbering corresponds to homologous yeast protein residues) does not form a complex with eIF4A (28, 29). However, none of these side chains contacts eIF4A directly and the effect of the triple mutation is most likely caused by a distortion of the structure. However, Ser-612 forms hydrogen bonds to eIF4A's

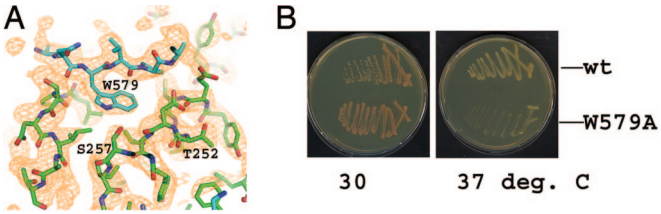

Fig. 5. Characterization of the W579A mutant. (*A*) Electron density around Trp-579. eIF4G C-atoms are cyan; eIF4A carbon atoms are green. Residues 577–582 were omitted from the phase calculation. The $2F_o$-F_c map is contoured at 1.0 standard deviations above the mean. (*B*) Temperature-sensitive phenotype of the *tif4631* W579A mutant. *In vivo* selection for yeast clones carrying the full-length W579A mutation was performed as described in *Materials and Methods*. The upper two sectors correspond to wild-type cells, the lower sector shows growth of the W579A mutant at 30°C (*Left*) and 37°C (*Right*).

Asp-256 and Thr-252. The amide side chain of the conserved Asn-615 forms two hydrogen bonds with eIF4A's main chain amide and carbonyl oxygen of Ile-257 and Val-259, respectively. The amino group of Lys-616 interacts with the carbonyl oxygen of Asp-282 and the aromatic side chain of Phe-284. The side chain of Thr-618 is hydrogen-bonded to the hydroxyl group of Thr-286 of eIF4A. The mutant T618I exhibits a temperature-sensitive phenotype (7) and the double mutation in human eIF4A-I (corresponding to KT284,286AK in yeast) shows no binding to eIF4G (10). eIF4A-Lys-284 forms a salt bridge with eIF4G-Glu-628 and with Asp-595.

The same surface patch involves eIF4G's Lys-655, Glu-659, and Tyr-666 (Fig. 4). These residues are directly involved in polar contacts to eIF4A; the glutamate and the tyrosine side chains form hydrogen bonds with eIF4A's conserved Arg-312. Single mutations of the latter two impair binding to eIF4A *in vitro* and the E659K mutant shows a slow-growth phenotype (7, 29). The double eIF4G double mutant SE612,659LK is lethal (7).

The second contiguous interaction surface involves the N-terminal domain of eIF4A and the C-terminal helix of eIF4G's middle domain. This contact involves Arg-835, which is close to eIF4A-Glu-43, and the exposed Phe-838 that fits snugly into a groove formed by eIF4A's Glu-31, Leu-34, Arg-35, and Phe-38.

Third Interaction Site Including Trp-579 Is Crucial for Complex Formation. N-terminal shortening of eIF4G (572–853) resulted in a significant loss of binding affinity, as was shown for eIF4G (592–862) (Fig. 2). Surprisingly, the N-terminal amino acids of eIF4G (572–853) were found to be mostly disordered in the crystal structure, the first clearly defined amino acid of eIF4G (572–853) being Leu-600. However, a peptide-shaped patch of positive difference electron density was visible in a hydrophobic groove on the surface of eIF4A-CTD, formed by Val-239, Val-241, Cys-250, Leu-254, Leu-386, and Ser-257. This unaccounted density could be interpreted as residues 577–582 of eIF4G. This segment contains the conserved Trp-579 residue (Fig. S2). Its side chain is buried in a pocket and forms a hydrogen bond to the hydroxyl group of Ser-257 of eIF4A (Fig. 5*A*).

To confirm this finding, we performed pull-down experiments with a mutant eIF4G protein where the conserved Trp-579 has been replaced by alanine. This mutant, referred to as eIF4G (572–853)(W579A), binds much more weakly to eIF4A than wild-type eIF4G (572–853), but more strongly than the truncated eIF4G (592–862) (Fig. 2 and Fig. S1). The importance of Trp-579 for its interaction with eIF4A was further corroborated by its weak enhancement of eIF4A ATPase activity by the mutant eIF4G (572–853)(W579A) (Fig. 3*A*, lane 7). Additionally, yeast cells carrying eIF4G1(W579A) as its sole source for eIF4G grow normally at 30°C but show a temperature-sensitive phenotype at 37°C (Fig. 5*B*).

Discussion

The solenoid eIF4G middle domain binds both the N-terminal and C-terminal domain of eIF4A. The two major interaction surfaces are approximately perpendicular to the surfaces bearing the DEAD-box motifs. eIF4A has an extended conformation that differs from all the ones described before, in that the important DEAD-box motifs still face each other.

To gain insight into the ATP-bound state of eIF4A, we modeled the closed conformation of yeast eIF4A by using the Vasa structure as a template [PDB ID code 2DB3 (22)] (Fig. S4). This implied a 42° rotation of eIF4A's N-terminal domain followed by some 10-Å shift. This conformational change drastically alters the distance between the RNA-interacting sequence motifs Ia and Ib, which are located in the N-terminal domain and motifs IV and V of the C-terminal domain, probably leading to a distortion of the bound RNA molecule and contributing to its unwinding. Assuming that the interaction surface on the eIF4A-CTD remains intact, modeling of the eIF4A–eIF4G complex in eIF4A's closed conformation reveals that the eIF4A-NTD is no longer in contact with eIF4G (Fig. S4). This model explains stimulation of eIF4A's ATPase activity by eIF4G. The latter acts as a "stopper," thus preventing eIF4A-NTD from moving too far and getting trapped in a nonproductive conformation, for example, by separating elements located on NTD and CTD. To examine this further, we have mutated the salt bridge Arg-35–Asp-842 between yeast eIF4A-NTD and eIF4G and used a C-terminally truncated human construct eIF4GI (710–970). Mutating Asp-842 for Arg does not have a significant effect on either binding (Fig. S1*D*) or ATPase activity (Fig. 3*A*, lane 5), whereas replacement of Arg-35 in eIF4A abolishes binding and ATPase stimulation (Fig. S1*E* and Fig. 3*A*, lanes 3 and 4). Elimination of the entire M4 motif in the human eIF4GI (710–970) protein does not significantly weaken its binding under gel filtration conditions (Fig. S1*F*) but results in a greatly diminished ATPase activity. This model differs from the "soft-clamp" proposed previously (10), which suggests that eIF4G stabilizes the closed conformation in the ATP state and does not contact eIF4A-NTD in the ADP state.

A third interaction site involves a flexible element in the N-terminal region of eIF4G middle domain. The key residue in this new interaction site is Trp-579, which is absolutely conserved among eIF4G-species (Fig. S2). Because the eIF4A–eIF4G interface is rather large, it is remarkable that the mutation of a single residue causes a significant decrease in its binding affinity for eIF4A and leads to a temperature-sensitive phenotype. Owing to its pocket shape and small surface, this new interaction site may well serve as target for the development of anticancer drugs.

mRNAs differ strongly in their translation efficiency, where those with long, structured 5′ UTRs have a much higher requirement for eIF4F (35). 5′ UTRs of this kind are present in several proto-oncogenes and somatic growth factors (36). Enhanced concentrations of eIF4F, for example, caused by misregulation of the TOR pathway (37) or by overexpression of eIF4E (38) or eIF4G (39) can lead to malignant cell development and growth. A possible strategy for anticancer drugs is therefore the development or identification of small-molecule compounds that are able to disrupt the eIF4F complex (40). Targeting protein–protein interactions with small molecules is usually difficult because of the large size and flatness of the surfaces involved and because most of the surface residues usually are not essential for binding (41, 42). However, eIF4G's Trp-579 interaction with the complementary pocket on the eIF4A surface could result in an efficient target for small molecules. This notion is supported by a recent publication on the translation inhibition by the anti-inflammatory and antineoplastic lipid mediator 15d-PGJ2, which binds covalently to Cys-264 of human eIF4A1,

a residue located in the vicinity the Trp-579 interaction site, thus disrupting the eIF4A–eIF4G complex (34).

Materials and Methods

Cloning, Expression and Purification. All constructs of eIF4A and eIF4G were amplified by PCR from a *S. cerevisiae* genomic DNA library or from a human cDNA library. PCR products were cut and ligated into the NdeI/XhoI sites of pET-28a vectors (Novagen). Yeast eIF4G (592–862), human eIF4GI (710–970), and human eIF4GI (710–1056) were cloned into a pGEX-6P1-vector (GE Life Sciences) by using the BamH1 and a EcoRI restriction sites. eIF4A was expressed in *Escherichia coli* BL21 Star (DE3) (Invitrogen), and eIF4G in *E. coli* BL21-CodonPlus (DE3)-RIL (Stratagene). Cells were induced with 1 mM isopropyl-thiogalactopyranoside (IPTG) for 12–20 h at 20°C. The expressed proteins were purified on Ni-NTA SUPERFLOW (Qiagen). $(His)_6$-tags were cleaved with thrombin (Amersham Bioscience). Single proteins were further purified by size exclusion chromatography (Superdex 75, Amersham Pharmacia) and by ion exchange chromatography (Resource Q). The eIF4G1(W579A) and the eIF4G (572–853)(W579A) constructs were generated by using an overlap-extension protocol (43) with primers 5′-GCTAATAGGGCGGTACCAAAATTC-AAGTCTAAAAAGACTG-3′ and 5′-GAATTTTGGTACCGCCCTATTAGCACTTGG-AACAAGTG-3′. eIF4G (572–853) (D842R) used primers 5′-GTTCAAGCTTATCCGTATTAAAGAATTAAGGCA-CGACAAGAAC-3′ and 5′TTTAATACGGATAAGCTTGAACTTGATTCTACTAGAAA-TCTTAGC-3′. For eIF4A(R35D) 5′-GACGAAAACCTTCTAGATGGTGTTTTCG-GTTACGGTTTCGAAG-3′ and 5′-GAAAACACCATCTAGAAGGTTTTCGTCCAA-TTCCATATCATCG-3′ were used.

Complex Formation. The complex was prepared by mixing the components in a 1:1 stoichiometric ratio and purified by size exclusion chromatography. All fractions were examined by dynamic light scattering (DLS). Fractions with a polydispersity index $<20\%$ were pooled and used for crystallization.

Pull-down Experiments. Two hundred microliters of Ni-NTA-Sepharose (Sigma) resin was incubated with 0.2 mg of his-tagged eIF4A and washed with a buffer containing 50 mM NaCl, 20 mM Tris·HCl (pH 7.4), and 10 mM imidazole. eIF4G proteins were added and incubated for 5 min on ice. The resin was then washed with 3 ml of buffer. Bound proteins were eluted with elution buffer (1.5 ml of 50 mM NaCl, 20 mM Tris·HCl, pH 7.4, 80 mM imidazole).

ATPase Activity Assay. To measure the release of inorganic phosphate, the EnzCheck assay (Invitrogen) was performed (44). Activity of yeast eIF4A (0.6 μM) was tested in the presence of RNA [either yeast whole RNA or poly(U) (Sigma-Aldrich) 150 μg/ml] and ATP (1.0 mM) and different eIF4G protein (1.5 μM) at 22°C.

***In Vivo* Experiments.** Yeast strain CBY19 (MATa ade2 trp1 leu2 ura3 his3 tif4631::LEU2 tif4632::ura3 ⟨Ycp50; TIF4631⟩), which expresses the essential eIF4G-activity from a centromeric plasmid carrying the URA3 gene as a selectable marker (⟨Ycp50; TIF4631⟩) (45), was transformed with plasmids pRS313-TIF4631wt or pRS313-tif4631W579A (both carry HIS3 as a selectable marker) and His^+-prototrophs selected on minimal medium YNB plates (2% glucose; +20 μg/ml adenine and tryptophan). Transformed cells that lost the URA3-plasmid ⟨Ycp50; TIF4631⟩ were selected on minimal medium YNB-plates containing 5-FOA (5-fluoro-orotic acid; 0.5 mg/ml), plated on full YPD medium (+2% glucose) and tested for their capability to grow at different temperatures (18°C, 30°C, and 37°C).

Crystallization, Data Collection, Structure Solution, and Refinement. Crystals were obtained at 277 K by vapor diffusion of 10–20 mg/ml complex against a reservoir of 0.2 M potassium sodium tartrate tetrahydrate (pH 7.2), 20% (wt/vol) PEG 3350, and 10 mM AMP or ADP. After cryoprotection by 20% glycerol, in-house data were collected on a Rigaku RU300 anode with a RaxisIV detector (Rigaku/MSC). Synchrotron data were collected at European Synchrotron Radiation Facility, Grenoble, at beamline ID29 with an ADSC Q315 CCD detector. At the synchrotron, crystals were annealed by blocking the cryostream for 4 s. Data were processed with HKL2000 (46) or XDS (47). Molecular replacement calculations were performed by using the program PHASER (48) and PDB ID codes 1QDE (14), 1FUK (19), and 1HU3 (5) as search models. The model was rebuilt by using the program COOT (49) and refined with PHENIX (50).

ACKNOWLEDGMENTS. We thank Christoph Muller-Dieckmann and Gordon Leonard for their help during data collection at European Synchrotron Radiation Facility, Grenoble, and Bernhard Erni for stimulating discussions and reading the manuscript. This work was supported by the Swiss National Science Foundation, the Berner Hochschulstiftung, and the University of Bern.

1. Dever TE (1999) Translation initiation: Adept at adapting. *Trends Biochem Sci* 24:398–403.
2. Kozak M (2002) Pushing the limits of the scanning mechanism for initiation of translation. *Gene* 299:1–34.
3. Merrick WC (2004) Cap-dependent and cap-independent translation in eukaryotic systems. *Gene* 332:1–11.
4. Bellsolell L, Cho-Park PF, Poulin F, Sonenberg N, Burley SK (2006) Two structurally atypical HEAT domains in the C-terminal portion of human eIF4G support binding to eIF4A and Mnk1. *Structure* 14:913–923.
5. Marcotrigiano J, *et al.* (2001) A conserved HEAT domain within eIF4G directs assembly of the translation initiation machinery. *Mol Cell* 7:193–203.
6. Dominguez D, Altmann M, Benz J, Baumann U, Trachsel H (1999) Interaction of translation initiation factor eIF4G with eIF4A in the yeast Saccharomyces cerevisiae. *J Biol Chem* 274:26720–26726.
7. Dominguez D, Kislig E, Altmann M, Trachsel H (2001) Structural and functional similarities between the central eukaryotic initiation factor (eIF)4A-binding domain of mammalian eIF4G and the eIF4A-binding domain of yeast eIF4G. *Biochem J* 355:223–230.
8. Linder P, *et al.* (1989) Birth of the D-E-A-D box. *Nature* 337:121–122.
9. Hinton TM, Coldwell MJ, Carpenter GA, Morley SJ, Pain VM (2007) Functional analysis of individual binding activities of the scaffold protein eIF4G. *J Biol Chem* 282:1695–1708.
10. Oberer M, Marintchev A, Wagner G (2005) Structural basis for the enhancement of eIF4A helicase activity by eIF4G. *Genes Dev* 19:2212–2223.
11. Pause A, Methot N, Svitkin Y, Merrick WC, Sonenberg N (1994) Dominant negative mutants of mammalian translation initiation factor eIF-4A define a critical role for eIF-4F in cap-dependent and cap-independent initiation of translation. *EMBO J* 13:1205–1215.
12. Korneeva NL, First EA, Benoit CA, Rhoads RE (2005) Interaction between the NH2-terminal domain of eIF4A and the central domain of eIF4G modulates RNA-stimulated ATPase activity. *J Biol Chem* 280:1872–1881.
13. Cordin O, Banroques J, Tanner NK, Linder P (2006) The DEAD-box protein family of RNA helicases. *Gene* 367:17–37.
14. Benz J, Trachsel H, Baumann U (1999) Crystal structure of the ATPase domain of translation initiation factor 4A from Saccharomyces cerevisiae—The prototype of the DEAD box protein family. *Structure* 7:671–679.
15. Cordin O, Tanner NK, Doere M, Linder P, Banroques J (2004) The newly discovered Q motif of DEAD-box RNA helicases regulates RNA-binding and helicase activity. *EMBO J* 23:2478–2487.
16. Tanner NK, Cordin O, Banroques J, Doere M, Linder P (2003) The Q motif: A newly identified motif in DEAD box helicases may regulate ATP binding and hydrolysis. *Mol Cell* 11:127–138.
17. Pause A, Sonenberg N (1992) Mutational analysis of a DEAD box RNA helicase: The mammalian translation initiation factor eIF-4A. *EMBO J* 11:2643–2654.
18. Andersen CB, *et al.* (2006) Structure of the exon junction core complex with a trapped DEAD-box ATPase bound to RNA. *Science* 313:1968–1972.
19. Caruthers JM, Johnson ER, McKay DB (2000) Crystal structure of yeast initiation factor 4A, a DEAD-box RNA helicase. *Proc Natl Acad Sci USA* 97:13080–13085.
20. Johnson E R, McKay DB (1999) Crystallographic structure of the amino terminal domain of yeast initiation factor 4A, a representative DEAD-box RNA helicase. *RNA* 5:1526–1534.
21. Bono F, Ebert J, Lorentzen E, Conti E (2006) The crystal structure of the exon junction complex reveals how it maintains a stable grip on mRNA. *Cell* 126:713–725.
22. Sengoku T, Nureki O, Nakamura A, Kobayashi S, Yokoyama S (2006) Structural basis for RNA unwinding by the DEAD-box protein Drosophila Vasa. *Cell* 125:287–300.
23. Story RM, Li H, Abelson JN (2001) Crystal structure of a DEAD box protein from the hyperthermophile Methanococcus jannaschii. *Proc Natl Acad Sci USA* 98:1465–1470.
24. Pause A, Methot N, Sonenberg N (1993) The HRIGRXXR region of the DEAD box RNA helicase eukaryotic translation initiation factor 4A is required for RNA binding and ATP hydrolysis. *Mol Cell Biol* 13:6789–6798.
25. Elles L M, Uhlenbeck OC (2008) Mutation of the arginine finger in the active site of Escherichia coli DbpA abolishes ATPase and helicase activity and confers a dominant slow growth phenotype. *Nucleic Acids Res* 36:41–50.
26. Marintchev A, Wagner G (2004) Translation initiation: Structures, mechanisms and evolution. *Q Rev Biophys* 37:197–284.
27. Sonenberg N, Dever TE (2003) Eukaryotic translation initiation factors and regulators. *Curr Opin Struct Biol* 13:56–63.
28. Imataka H, Sonenberg N (1997) Human eukaryotic translation initiation factor 4G (eIF4G) possesses two separate and independent binding sites for eIF4A. *Mol Cell Biol* 17:6940–6947.
29. Morino S, Imataka H, Svitkin YV, Pestova TV, Sonenberg N (2000) Eukaryotic translation initiation factor 4E (eIF4E) binding site and the middle one-third of eIF4GI constitute the core domain for cap-dependent translation, and the C-terminal one-third functions as a modulatory region. *Mol Cell Biol* 20:468–477.
30. Neff C L, Sachs AB (1999) Eukaryotic translation initiation factors 4G and 4A from Saccharomyces cerevisiae interact physically and functionally. *Mol Cell Biol* 19:5557–5564.
31. Zakowicz H, *et al.* (2005) Mutational analysis of the DEAD-box RNA helicase eIF4AII characterizes its interaction with transformation suppressor Pdcd4 and eIF4GI. *RNA* 11:261–274.
32. Lovell SC, Word JM, Richardson JS, Richardson DC (1999) Asparagine and glutamine rotamers: B-factor cutoff and correction of amide flips yield distinct clustering. *Proc Natl Acad Sci USA* 96:400–405.

33. Prat A, *et al.* (1990) Expression of translation initiation factor 4A from yeast and mouse in Saccharomyces cerevisiae. *Biochim Biophys Acta* 1050:140–145.
34. Kim WJ, Kim JH, Jang SK (2007) Anti-inflammatory lipid mediator 15d-PGJ2 inhibits translation through inactivation of eIF4A. *EMBO J* 26:5020–5032.
35. Pickering B M, Willis AE (2005) The implications of structured 5′ untranslated regions on translation and disease. *Semin Cell Dev Biol* 16:39–47.
36. Zimmer SG, DeBenedetti A, Graff JR (2000) Translational control of malignancy: The mRNA cap-binding protein, eIF-4E, as a central regulator of tumor formation, growth, invasion and metastasis. *Anticancer Res* 20:1343–1351.
37. Lee CH, Inoki K, Guan KL (2007) mTOR pathway as a target in tissue hypertrophy. *Annu Rev Pharmacol Toxicol* 47:443–467.
38. Avdulov S, *et al.* (2004) Activation of translation complex eIF4F is essential for the genesis and maintenance of the malignant phenotype in human mammary epithelial cells. *Cancer Cell* 5:553–563.
39. Fukuchi-Shimogori T, *et al.* (1997) Malignant transformation by overproduction of translation initiation factor eIF4G. *Cancer Res* 57:5041–5044.
40. Moerke NJ, *et al.* (2007) Small-molecule inhibition of the interaction between the translation initiation factors eIF4E and eIF4G. *Cell* 128:257–267.
41. Hershberger SJ, Lee SG, Chmielewski J (2007) Scaffolds for blocking protein-protein interactions. *Current Top Med Chem* 7:928–942.
42. Ofran Y, Rost B (2007) Protein-protein interaction hotspots carved into sequences. *PLoS Comput Biol* 3:e119.
43. Zheng L, Baumann U, Reymond JL (2004) An efficient one-step site-directed and site-saturation mutagenesis protocol. *Nucleic Acids Res* 32:e115.
44. Webb MR (1992) A continuous spectrophotometric assay for inorganic phosphate and for measuring phosphate release kinetics in biological systems. *Proc Natl Acad Sci USA* 89:4884–4887.
45. Berset C, Trachsel H, Altmann M (1998) The TOR (target of rapamycin) signal transduction pathway regulates the stability of translation initiation factor eIF4G in the yeast Saccharomyces cerevisiae. *Proc Natl Acad Sci USA* 95:4264–4269.
46. Otwinowski Z, Minor W (1997) Processing of X-ray diffraction data collected in oscillation mode. *Methods Enzymol* 276:307–326.
47. Kabsch W (2001) *International Tables for Crystallography*, eds Rossmann MG, Arnold E (Kluwer Academic Publisher, Dordrecht), Vol F, pp 730–734.
48. McCoy AJ, Grosse-Kunstleve RW, Storoni LC, Read RJ (2005) Likelihood-enhanced fast translation functions. *Acta Crystallogr D Biol Crystallogr* 61:458–464.
49. Emsley P, Cowtan K (2004) Coot: Model-building tools for molecular graphics. *Acta Crystallogr D Biol Crystallogr* 60:2126–2132.
50. Adams PD, *et al.* (2002) PHENIX: Building new software for automated crystallographic structure determination. *Acta Crystallogr D Biol Crystallogr* 58:1948–1954.